18th International Conference on the Application of Computer
Science and Mathematics in Architecture and Civil Engineering
K. Gürlebeck and C. Könke (eds.)
Weimar, Germany, 07–09 July 2009

A SMOOTHED FINITE ELEMENT METHOD FOR THE STATIC AND FREE VIBRATION ANALYSIS OF SHELLS

Nhon Nguyen*, **Timon Rabczuk**

**Institute of Structural Mechanics*
Bauhaus-University Weimar,
Marienstrasse 15,
D-99423 Weimar
E-mail: timon.rabczuk@uni-weimar.de
nhon.nguyen.thanh@uni-weimar.de

Keywords: Shell element, MITC4 elements, Smoothed finite elements method (SFEM).

Abstract. *A four-node quadrilateral shell element with smoothed membrane-bending based on Mindlin-Reissner theory is proposed. The element is a combination of a plate bending and membrane element. It is based on mixed interpolation where the bending and membrane stiffness matrices are calculated on the boundaries of the smoothing cells while the shear terms are approximated by independent interpolation functions in natural coordinates. The proposed element is robust, computationally inexpensive and free of locking. Since the integration is done on the element boundaries for the bending and membrane terms, the element is more accurate than the MITC4 element for distorted meshes. This will be demonstrated for several numerical examples.*

1 INTRODUCTION

The static and free vibration analysis of shell structures plays an important role in engineering applications as shells are widely used as structural components. Due to limitations of analytical methods [45,23,22,12] for practical applications, numerical methods have become the most widely used tool for designing shell structures. One of the most popular numerical approaches for analyzing vibration characteristics of shells is the Finite Element Method (FEM).

Although the FEM provides a general and systematic technique for constructing basis functions, a number of difficulties still exist in the development of shell elements based on shear deformation theories. One is the shear locking phenomenon for low order displacement models based on Mindlin Reissner theory [38, 27] as the shell thickness decreases. Membrane locking also occurs for shell elements and curved geometries. In order to avoid this drawback, various improvements and numerical techniques have been developed, e.g. reduced and selective integration elements [16,46], mixed formulation/hybrid elements [35], the Assumed Natural Strain (ANS) method [15, 2, 3, 10] and Enhanced Assumed Strain (EAS) method [41, 39, 8, 7]. Many improved shell elements have been developed [37, 36, 6, 42, 43, 14] and can be found in the textbooks [1,46].

Recently, this smoothing technique was incorporated into the FEM, leading to the smoothed finite element method (SFEM) proposed by Liu *et al*. [25]. It was shown by numerical examples that the SFEM is very robust, accurate and computational inexpensive, [26, 31, 30]. As we will show by several numerical examples, the proposed shell element is especially useful for distorted elements.

The paper is organized as follows: In the next section, we will state the formulation shell element formulation. Section 3 describes the smoothing technique in order to evaluate the bending and membrane stiffness. Section 4 discusses several numerical examples that are compared to analytical solutions and other elements from the literature. Finally, we close our paper with some concluding remarks.

2 FORMULATIONS FOR QUADRILATERAL SHELL ELEMENT

A typical Mindlin-Reissner shell with notations shown in figure 1 is considered here. For an initially flat isotropic thick shell, the membrane deformations are accounted for since they are uncoupled from the bending and shear deformations. Hence, the basic assumptions for the displacement behavior [13] are:

$$\begin{aligned} u(x,y,z) &= u^0(x,y) + z\beta_x(x,y) \\ v(x,y,z) &= v^0(x,y) + z\beta_y(x,y) \\ w(x,y,z) &= w^0(x,y) \end{aligned} \tag{1}$$

where u^0, v^0, w^0 are displacement components in the x, y, z directions (local coordinate system), respectively. β_x and β_y are the rotations of the normal to the undeformed mid-surface in the xz and yz planes, respectively, $\beta_x = \frac{\partial w}{\partial x}$ and $\beta_y = \frac{\partial w}{\partial y}$.
The membrane $\boldsymbol{\varepsilon}^m$ and curvature strains $\boldsymbol{\kappa}$ are defined as

$$\boldsymbol{\varepsilon}^m = \begin{bmatrix} \frac{\partial u_0}{\partial x} \\ \frac{\partial v_0}{\partial y} \\ \frac{\partial u_0}{\partial y} + \frac{\partial v_0}{\partial x} \end{bmatrix}, \qquad \boldsymbol{\kappa} = \begin{bmatrix} \frac{\partial \beta_x}{\partial x} \\ -\frac{\partial \beta_y}{\partial y} \\ \frac{\partial \beta_x}{\partial y} - \frac{\partial \beta_y}{\partial x} \end{bmatrix} \tag{2}$$

and the transverse shear strain vector is

$$\boldsymbol{\gamma} = \left\{ \begin{array}{c} \gamma_{xz} \\ \gamma_{yz} \end{array} \right\} = \left\{ \begin{array}{c} \frac{\partial w}{\partial x} + \beta_x \\ \frac{\partial w}{\partial y} - \beta_y \end{array} \right\} \tag{3}$$

By means of the spatial discretization procedure in the FEM, the displacement and strains within any element can be written as

$$\mathbf{u}^h = \sum_{i=1}^{np} \left[\begin{array}{cccccc} N_i & 0 & 0 & 0 & 0 & 0 \\ 0 & N_i & 0 & 0 & 0 & 0 \\ 0 & 0 & N_i & 0 & 0 & 0 \\ 0 & 0 & 0 & 0 & N_i & 0 \\ 0 & 0 & 0 & N_i & 0 & 0 \\ 0 & 0 & 0 & 0 & 0 & 0 \end{array} \right] \mathbf{q}_i \tag{4}$$

where $\mathbf{q}_i = \left\{ \begin{array}{cccccc} u_i & v_i & w_i & \theta_{xi} & \theta_{yi} & \theta_{zi} \end{array} \right\}^T$ is the nodal displacement vector

$$\boldsymbol{\varepsilon}^m = \sum_i \mathbf{B}_i^m \mathbf{q}_i \;; \qquad \boldsymbol{\kappa} = \sum_i \mathbf{B}_i^b \mathbf{q}_i \;; \qquad \boldsymbol{\gamma} = \sum_i \mathbf{B}_i^s \mathbf{q}_i \tag{5}$$

$$\mathbf{B}_i^m = \left[\begin{array}{cccccc} N_{i,x} & 0 & 0 & 0 & 0 & 0 \\ 0 & N_{i,y} & 0 & 0 & 0 & 0 \\ N_{i,y} & N_{i,x} & 0 & 0 & 0 & 0 \end{array} \right] \;; \qquad \mathbf{B}_i^b = \left[\begin{array}{cccccc} 0 & 0 & 0 & 0 & N_{i,x} & 0 \\ 0 & 0 & 0 & -N_{i,x} & 0 & 0 \\ 0 & 0 & 0 & -N_{i,x} & N_{i,y} & 0 \end{array} \right] \tag{6}$$

$$\mathbf{B}_i^s = \left[\begin{array}{cccccc} 0 & 0 & N_{i,x} & 0 & N_i & 0 \\ 0 & 0 & N_{i,y} & -N_i & 0 & 0 \end{array} \right] \tag{7}$$

As known in References [47, 17, 19], the use of reduced integration on the shear term $\mathbf{k}^s$ can avoid shear locking as the thickness of the shell tends to zero. However, these elements fail the patch test and exhibit an instability due to rank deficiency [31]. In order to improve these elements, we use independent interpolation fields in the natural coordinate system for the approximation of the shear strains [2].

$$\left[\begin{array}{c} \gamma_x \\ \gamma_y \end{array} \right] = \mathbf{J}^{-1} \left[\begin{array}{c} \gamma_\xi \\ \gamma_\eta \end{array} \right] \tag{8}$$

where

$$\gamma_\xi = \frac{1}{2}[(1-\eta)\gamma_\xi^B + (1+\eta)\gamma_\xi^D],\ \gamma_\eta = \frac{1}{2}[(1-\xi)\gamma_\eta^A + (1+\xi)\gamma_\eta^C] \tag{9}$$

where $\mathbf{J}$ is the Jacobian matrix and the mid-side nodes A, B, C, D are shown in figure 1. In case of bending around the η-axis, it is useful to place the sampling points at positions $\xi = 0$ where the parasitic transverse shear strains vanish. We recall, that γ_ξ linearly varies in ξ - direction. In order to retain a linear variation of γ_ξ in η - direction, we choose two sampling points, at $\xi = 0$, $\eta = 1$ and at $\xi = 0$, $\eta = -1$ (points A and C). For the transverse shear strains γ_η we proceed in a similar way (points B and D). Presenting $\gamma_\xi^B, \gamma_\xi^D$ and $\gamma_\eta^A, \gamma_\eta^C$ based on the discretized fields u^h, we obtain the shear matrix:

$$\mathbf{B}_i^s = \mathbf{J}^{-1} \left[\begin{array}{cccccc} 0 & 0 & N_{i,\xi} & -b_i^{12} N_{i,\xi} & b_i^{11} N_{i,\xi} & 0 \\ 0 & 0 & N_{i,\eta} & -b_i^{22} N_{i,\eta} & b_i^{21} N_{i,\eta} & 0 \end{array} \right] \tag{10}$$

where

$$b_i^{11} = \xi_i x^M_{,\xi}\,,\; b_i^{12} = \xi_i y^M_{,\xi}\,,\;\; b_i^{21} = \eta_i x^L_{,\eta},\;\; b_i^{22} = \eta_i y^L_{,\eta} \tag{11}$$

with $\xi_i \in \{-1, 1, 1, -1\}$, $\eta_i \in \{-1, -1, 1, 1\}$ and $(i, M, L) \in \{(1, B, A); (2, B, C); (3, D, C); (4, D, A)\}$.

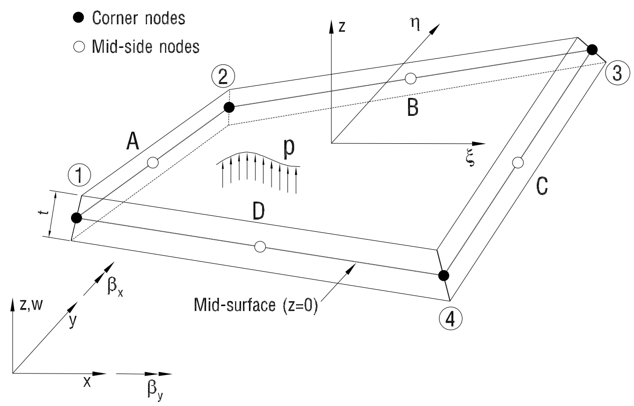

Figure 1: Quadrilateral shell element.

The formulation for the free vibration of a Mindlin-Reissner shell can be written in matrix form as

$$\mathbf{m}^e \ddot{\mathbf{q}} + \mathbf{k}^e \mathbf{q} = \mathbf{0} \tag{12}$$

where

$$\mathbf{k}^e = \int\limits_{\Omega^e} (\mathbf{B}^m)^T \mathbf{D}^m B^m d\Omega + \int\limits_{\Omega^e} \left(\mathbf{B}^b\right)^T \mathbf{D}^b \mathbf{B}^b d\Omega + \int\limits_{\Omega^e} (\mathbf{B}^s)^T \mathbf{D}^s \mathbf{B}^s d\Omega \tag{13}$$

$$\mathbf{m}^e = \int\limits_{\Omega^e} \mathbf{N}^T \mathbf{m} \mathbf{N} d\Omega \qquad \text{with} \quad \mathbf{m} = \rho \begin{bmatrix} t & 0 & 0 & 0 & 0 & 0 \\ 0 & t & 0 & 0 & 0 & 0 \\ 0 & 0 & t & 0 & 0 & 0 \\ 0 & 0 & 0 & 0 & \frac{t^3}{12} & 0 \\ 0 & 0 & 0 & \frac{t^3}{12} & 0 & 0 \\ 0 & 0 & 0 & 0 & 0 & 0 \end{bmatrix} \tag{14}$$

and

$$\mathbf{D}^m = \frac{Et}{(1-\nu)^2} \begin{bmatrix} 1 & \nu & 0 \\ \nu & 1 & 0 \\ 0 & 0 & \frac{1-\nu}{2} \end{bmatrix}, \;\; \mathbf{D}^b = \frac{Et^3}{12\,(1-\nu)^2} \begin{bmatrix} 1 & \nu & 0 \\ \nu & 1 & 0 \\ 0 & 0 & \frac{1-\nu}{2} \end{bmatrix} \tag{15}$$

$$\mathbf{D}^s = \frac{kEt}{2\,(1+\nu)} \begin{bmatrix} 1 & 0 \\ 0 & 1 \end{bmatrix} \tag{16}$$

The transformation between global coordinates and local coordinates is required to generate the local element stiffness matrix in the local coordinate system.

$$\left\{ \begin{array}{c} u \\ v \\ w \end{array} \right\} = \mathbf{T}_l \left\{ \begin{array}{c} U \\ V \\ W \end{array} \right\} \quad \text{and} \quad \left\{ \begin{array}{c} \theta_{\mathrm{x}} \\ \theta_{\mathrm{y}} \\ \theta_{\mathrm{z}} \end{array} \right\} = \mathbf{T}_l \left\{ \begin{array}{c} \theta_{\mathrm{X}} \\ \theta_{\mathrm{Y}} \\ \theta_{\mathrm{Z}} \end{array} \right\} \tag{17}$$

where $\mathbf{T}_l$ is the transformation matrix as given in [46]. Finally, the element stiffness $\mathbf{K}$, mass $\mathbf{M}$ in the global coordinate system, can be written as

$$\mathbf{K} = \bar{\mathbf{T}}^T \mathbf{k}^e \bar{\mathbf{T}}, \quad \mathbf{M} = \bar{\mathbf{T}}^T \mathbf{m}^e \bar{\mathbf{T}} \tag{18}$$

where

$$\bar{\mathbf{T}} = \begin{bmatrix} T_l & & & & & \\ & T_l & & & & \\ & & T_l & & & \\ & & & T_l & & \\ & & & & T_l & \\ & & & & & T_l \end{bmatrix} \tag{19}$$

3 A MIXED INTERPOLATION AND A SMOOTHED METHOD FOR FOUR-NODE QUADRILATERAL SHELL ELEMENT

The strain smoothing method was proposed by [9]. A strain smoothing stabilization is created to compute the nodal strain as the divergence of a spatial average of the strain field. This strain smoothing avoids evaluating derivatives of mesh-free shape functions at nodes and thus eliminates defective modes. The motivation of this work is to develop the strain smoothing approach for the FEM. The method developed here can be seen as a stabilized conforming nodal integration method, as in Galerkin mesh-free methods applied to the finite element method. The smooth strain field at an arbitrary point $\mathbf{x}_C$ is written as

$$\tilde{\varepsilon}_{ij}(\mathbf{x}_C) = \int_{\Omega^h} \varepsilon_{ij}(\mathbf{x})\, \Phi(\mathbf{x} - \mathbf{x}_C)\, d\Omega \tag{20}$$

where Φ is a smoothing function that satisfies the following properties

$$\Phi \geq 0 \qquad \text{and} \qquad \int_{\Omega^h} \Phi d\Omega = 1 \tag{21}$$

For simplicity, Φ is assumed to be a step function defined by

$$\Phi(\mathbf{x} - \mathbf{x}_C) = \begin{cases} 1/A_C, \mathbf{x} \in \Omega_C \\ 0, \mathbf{x} \notin \Omega_C \end{cases} \tag{22}$$

where A_C is the area of the smoothing cell, $\Omega_C \subset \Omega^e \subset \Omega^h$, as shown in figure 2.
Substituting Eq. (22) into Eq. (20), and applying the divergence theorem, we obtain

$$\tilde{\varepsilon}_{ij}(\mathbf{x}_C) = \frac{1}{2A_C} \int_{\Omega_C} \left(\frac{\partial u_i}{\partial x_j} + \frac{\partial u_j}{\partial x_i} \right) d\Omega = \frac{1}{2A_C} \int_{\Gamma_C} (u_i n_j + u_j n_j)\, d\Gamma \tag{23}$$

Next, we consider an arbitrary smoothing cell, Ω_C illustrated in figure 2 with boundary $\Gamma_C = \bigcup_{b=1}^{nb} \Gamma_C^b$, where Γ_C^b is the boundary segment of Ω_C, and nb is the total number of edges of each smoothing cell. The relationship between the strain field and the nodal displacement is rewritten as

$$\tilde{\boldsymbol{\varepsilon}} = \left\{ \begin{array}{c} \tilde{\boldsymbol{\kappa}} \\ \tilde{\boldsymbol{\varepsilon}}^m \end{array} \right\} \tag{24}$$

where

$$\begin{aligned}\tilde{\boldsymbol{\kappa}} &= \tilde{\mathbf{B}}_C^b \mathbf{q} \\ \tilde{\boldsymbol{\varepsilon}}^m &= \tilde{\mathbf{B}}_C^m \mathbf{q}\end{aligned} \tag{25}$$

The smoothed element membrane and bending stiffness matrix is obtained by

$$\tilde{\mathbf{k}}_m^e = \int_{\Omega^e} (\tilde{\mathbf{B}}_C^m)^T \mathbf{D}^m \tilde{\mathbf{B}}_C^m d\Omega = \sum_{C=1}^{nc} (\tilde{\mathbf{B}}_C^m)^T (\mathbf{x}_C) \mathbf{D}^m \tilde{\mathbf{B}}_C^m (\mathbf{x}_C) A_C \tag{26}$$

$$\tilde{\mathbf{k}}_b^e = \int_{\Omega^e} (\tilde{\mathbf{B}}_C^b)^T \mathbf{D}^b \tilde{\mathbf{B}}_C^b d\Omega = \sum_{C=1}^{nc} (\tilde{\mathbf{B}}_C^b)^T (\mathbf{x}_C) \mathbf{D}^b \tilde{\mathbf{B}}_C^b (\mathbf{x}_C) A_C \tag{27}$$

where nc is the number of smoothing cells of the element, see figure 3.
The integrands are constant over each Ω_C and the non-local strain displacement matrix reads

$$\tilde{\mathbf{B}}_{C_i}^m (\mathbf{x}_C) = \frac{1}{A_C} \int_{\Gamma_C} \begin{pmatrix} N_i n_x & 0 & 0 & 0 & 0 & 0 \\ 0 & N_i n_y & 0 & 0 & 0 & 0 \\ N_i n_y & N_i n_x & 0 & 0 & 0 & 0 \end{pmatrix} d\Gamma \tag{28}$$

$$\tilde{\mathbf{B}}_{Ci}^b (\mathbf{x}_C) = \frac{1}{A_C} \int_{\Gamma_C} \begin{pmatrix} 0 & 0 & 0 & 0 & N_i n_x & 0 \\ 0 & 0 & 0 & -N_i n_y & 0 & 0 \\ 0 & 0 & 0 & -N_i n_x & N_i n_y & 0 \end{pmatrix} d\Gamma \tag{29}$$

From Eq. (29), we can use Gauss points for line integration along each segment of Γ_C^b. If the shape functions are linear on each segment of a cell's boundary, one Gauss point is sufficient for an exact integration:

$$\tilde{\mathbf{B}}_{C_i}^m (\mathbf{x}_C) = \frac{1}{A_C} \sum_{b=1}^{nb} \begin{pmatrix} N_i \left(\mathbf{x}^G\right) n_x & 0 & 0 & 0 & 0 & 0 \\ 0 & N_i \left(\mathbf{x}^G\right) n_y & 0 & 0 & 0 & 0 \\ N_i \left(\mathbf{x}^G\right) n_y & N_i \left(\mathbf{x}^G\right) n_x & 0 & 0 & 0 & 0 \end{pmatrix} l_b^C \tag{30}$$

$$\tilde{\mathbf{B}}_{Ci}^b (\mathbf{x}_C) = \frac{1}{A_C} \sum_{b=1}^{nb} \begin{pmatrix} 0 & 0 & 0 & 0 & N_i(\mathbf{x}^G) n_x & 0 \\ 0 & 0 & 0 & -N_i(\mathbf{x}^G) n_y & 0 & 0 \\ 0 & 0 & 0 & -N_i(\mathbf{x}^G) n_x & N_i(\mathbf{x}^G) n_y & 0 \end{pmatrix} l_b^C \tag{31}$$

where $\mathbf{x}^G$ and l_b^C are the midpoint (Gauss point) and the length of Γ_b^C, respectively, and nb is the total number of edges of each smoothing cell.
The smoothed membrane and curvatures lead to high flexibility such as arbitrary polygonal elements, and a slight reduction in computational cost. The element is subdivided into nc non-overlapping sub-domains also called smoothing cells. figure 3 illustrates different smoothing cells for nc = 1, 2, and 4 corresponding to 1-subcell, 2-subcell, and 4-subcell methods. The membrane and curvature are smoothed over each sub-cell. The values of the shape functions are indicated at the corner nodes in figure 3 in the format (N_1, N_2, N_3, N_4). The values of the shape functions at the integration nodes are determined based on the linear interpolation of shape functions along boundaries of the element or the smoothing cells.
Hence, the element stiffness matrix and geometrical stiffness matrix write:

$$\tilde{\mathbf{k}}^e = \tilde{\mathbf{k}}_b^e + \tilde{\mathbf{k}}_m^e + \mathbf{k}_s^e \tag{32}$$

where

$$\tilde{\mathbf{k}}_b^e = \int_{\Omega^e} \tilde{\mathbf{B}}_b^T \mathbf{D} \tilde{\mathbf{B}}_b d\Omega = \sum_{C=1}^{nc} \left(\tilde{\mathbf{B}}_C^b\right)^T (\mathbf{x}_C) \mathbf{D}^b \tilde{\mathbf{B}}_C^b (\mathbf{x}_C) A_C \tag{33}$$

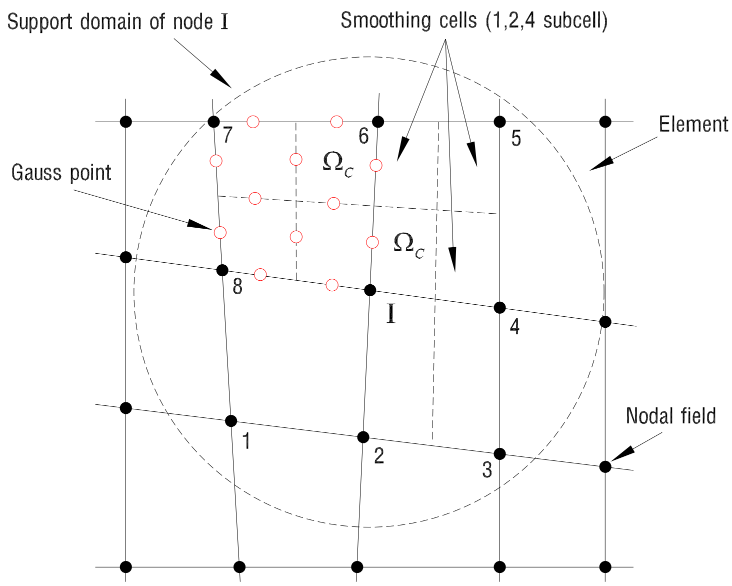

Figure 2: Example of finite element meshes and smoothing cells

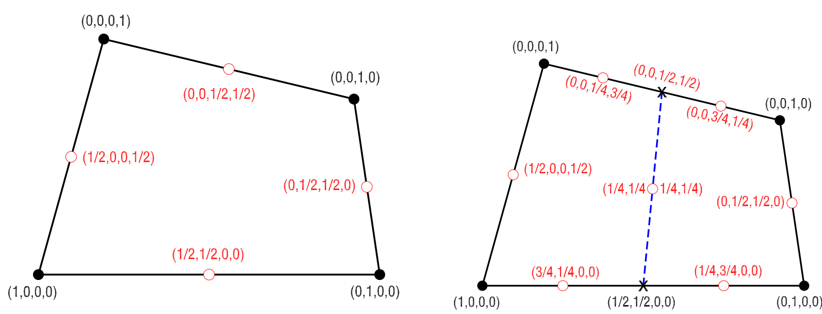

(a) 1-Subcell

(b) 2-Subcell

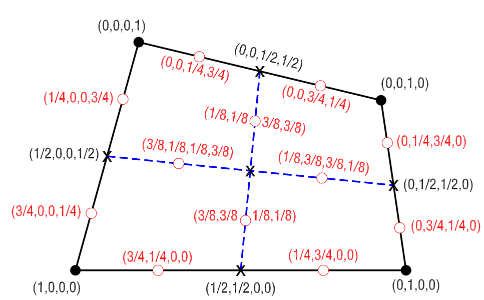

(c) 4-Subcell

Figure 3: Division of an element into smoothing cells (nc) and the value of the shape function along the boundaries of cells: k-Subcell stands for the shape function of the MISTk element, $k = 1, 2, 4$

$$\tilde{\mathbf{k}}_m^e = \int_{\Omega^e} \tilde{\mathbf{B}}_m^T \mathbf{D} \tilde{\mathbf{B}}_m d\Omega = \sum_{C=1}^{nc} \left(\tilde{\mathbf{B}}_C^m\right)^T (\mathbf{x}_C)\, \mathbf{D}^m \tilde{\mathbf{B}}_C^m (\mathbf{x}_C)\, A_C \tag{34}$$

$$\mathbf{k}_s^e = \int_{-1}^{1}\int_{-1}^{1} \mathbf{B}_s^T \mathbf{D}_s \mathbf{B}_s |\mathbf{J}|\, d\xi d\eta = \sum_{i=1}^{2}\sum_{j=1}^{2} w_i w_j \mathbf{B}_s^T \mathbf{D}_s \mathbf{B}_s |\mathbf{J}| \tag{35}$$

It is seen that the element membrane-bending and geometrical stiffness matrices are now constructed based on the smoothing operator on each smoothing cell of the element while the shear term $\mathbf{k}_s^e$ is derived from an interpolation independent from that of the shear strains, in the natural coordinates [2]. The shear contribution is therefore calculated as usual using Gauss quadrature and, in this paper, we use a 2 point rule.
The transformation of the element stiffness matrix and geometrical stiffness matrix from the local to the global coordinate system is given by

$$\left[\tilde{\mathbf{K}}\right]_{24\times24} = [\mathbf{T}]_{24\times24}^T \left[\tilde{\mathbf{k}}^e\right]_{24\times24} [\mathbf{T}]_{24\times24} \tag{36}$$

The final formulation of the free vibration of shells with the smoothed version reads:

$$\mathbf{M}\ddot{\mathbf{q}} + \tilde{\mathbf{K}}\mathbf{q} = \mathbf{0} \tag{37}$$

A general solution of such an equation can be written $\mathbf{q} = \bar{\mathbf{q}} \exp(i\omega t)$. Upon substitution of this general solution into Eq. (37), the frequency ω can be found by solving

$$\left(\tilde{\mathbf{K}} - \omega^2 \mathbf{M}\right) \bar{\mathbf{q}} = \mathbf{0} \tag{38}$$

where $\tilde{\mathbf{K}}$ is the global smoothed stiffness matrix, $\mathbf{M}$ is the global mass matrix, vector $\bar{\mathbf{q}}$ contains the vibration mode shapes, ω is the natural frequency.

4 NUMERICAL RESULTS

4.1 Static analysis

We name our element MISTk (Mixed Interpolation with Smoothing Technique with $k \in \{1, 2, 4\}$ related to number of smoothing cells as given by figure 3). For several numerical examples, we will now compare the MISTk elements to the widely used MITC4 elements. One major advantage of our element is that it is especially accurate for distorted meshes. To obtain mesh distortion that occurs naturally under phenomena such as shear bending or cracking, the coordinates of the initially regularly (structured) spaced interior nodes are relocated by the following expression [25]:

$$\begin{aligned} x' &= x + \alpha r_c \Delta x \\ y' &= y + \alpha r_c \Delta y \end{aligned} \tag{39}$$

where r_c is a random number between -1.0 and 1.0, $\alpha \in [0, 0.5]$ is used to control the shapes of the distorted elements and $\Delta x, \Delta y$ are initial regular element sizes in the x–and y–directions, respectively. In the next two sections, we did not disturb the y-direction in order to ensure smooth curvature.

4.1.1 Pinched cylinder with diaphragm

Consider a cylindrical shell with rigid end diaphragm subjected to a point load at the center of the cylindrical surface. Due to its symmetry, only one eighth of the cylinder shown in figure 4 is modeled. The expected deflection under a concentrated load is 1.8425×10^{-5} [44].
The problem is described with $N \times N$ MITC4 or MISTk elements in regular and irregular configurations. The meshes used are shown in figure 4.
Figure 5 and figure 6 illustrate the convergence of the displacement at the center point and the strain energy, respectively, for the MITC4 element and our MISTk elements for regular meshes. Our element is slightly more accurate than the MITC4 element for structured meshes. In table 1, we have compared the normalized displacement at the center point of our element to the MITC4 element. The strain energy is summarized in table 2.
The advantage of our element becomes more relevant for distorted meshes, see figure 7 – figure 8 and table 3 – table 4. For the same reasons as outlined in the previous section, the MISTk elements are significantly more accurate as compared to the MITC4-element with increasing mesh distortion.

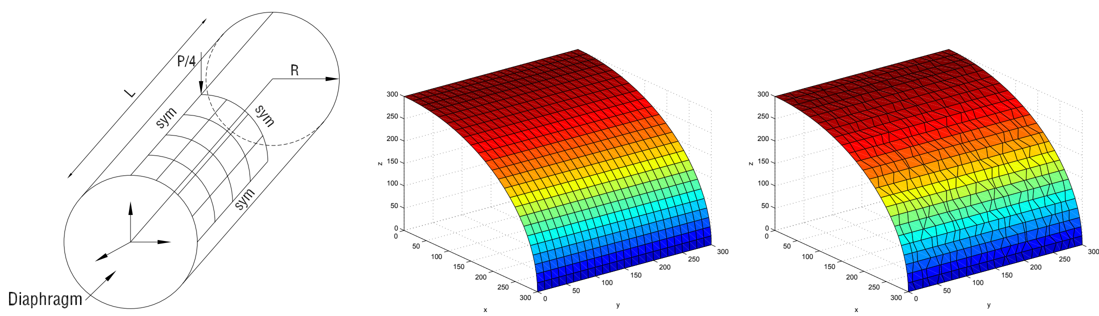

(a) Pinched cylinder (b) Regular meshes (c) Irregular meshes

Figure 4: Pinched cylinder with diaphragms boundary conditions (P = 1; R = 300; L = 600; t = 3; $\upsilon = 0.3$; E = 3×10^{7})

Table 1: Normal displacement under the load for a regular mesh

Mesh	MITC4	Mixed [40]	QPH [4]	SRI [18]	Present elements		
					MIST1	MIST2	MIST4
4×4	0.3677	0.399	0.370	0.373	0.4705	0.4376	0.3838
8×8	0.7363	0.763	0.740	0.747	0.8016	0.7802	0.7481
12×12	0.8656	-	-	-	0.9071	0.8935	0.8735
16×16	0.9203	0.935	0.930	0.935	0.9482	0.9391	0.9257
20×20	0.9481	-	-	-	0.9681	0.9616	0.9520
24×24	0.9644	-	-	-	0.9794	0.9745	0.9673

Table 2: The strain energy for a regular mesh

Mesh N^o	MITC4	Present elements		
		MIST1	MIST2	MIST4
4×4	8.4675e-7	1.0837e-6	1.0078e-6	8.8394e-7
8×8	1.6958e-6	1.8462e-6	1.7970e-6	1.7230e-6
12×12	1.9937e-6	2.0891e-6	2.0579e-6	2.0118e-6
16×16	2.1196e-6	2.1837e-6	2.1630e-6	2.1320e-6
20×20	2.1836e-6	2.2296e-6	2.2147e-6	2.1926e-6
24×24	2.2210e-6	2.2556e-6	2.2444e-6	2.2278e-6

Table 3: Normal displacement under the load for a irregular mesh

Mesh N^o	MITC4($\alpha = 0.5$)	MIST2				
		$\alpha = 0.1$	$\alpha = 0.2$	$\alpha = 0.3$	$\alpha = 0.4$	$\alpha = 0.5$
4×4	0.3539	0.4370	0.4342	0.4331	0.4261	0.4398
8×8	0.6950	0.7777	0.7786	0.7839	0.7803	0.7860
12×12	0.7402	0.8941	0.8938	0.8945	0.8959	0.8930
16×16	0.8488	0.9397	0.9394	0.9344	0.9402	0.9350
20×20	0.8960	0.9614	0.9631	0.9586	0.9628	0.9601
24×24	0.8718	0.9746	0.9739	0.9764	0.9755	0.9672

Table 4: The strain energy for a irregular mesh

Mesh N^o	MITC4($\alpha = 0.5$)	MIST2				
		$\alpha = 0.1$	$\alpha = 0.2$	$\alpha = 0.3$	$\alpha = 0.4$	$\alpha = 0.5$
4×4	8.1512e-7	1.0065e-6	1.0001e-6	9.9738e-7	9.8127e-7	1.0129e-6
8×8	1.6007e-6	1.7911e-6	1.7932e-6	1.8054e-6	1.7971e-6	1.8102e-6
12×12	1.7047e-6	2.0591e-6	2.0585e-6	2.0601e-6	2.0634e-6	2.0567e-6
16×16	1.9549e-6	2.1642e-6	2.1636e-6	2.1521e-6	2.1654e-6	2.1534e-6
20×20	2.0636e-6	2.2142e-6	2.2182e-6	2.2077e-6	2.2175e-6	2.2113e-6
24×24	2.0078e-6	2.2445e-6	2.2431e-6	2.2488e-6	2.2466e-6	2.2276e-6

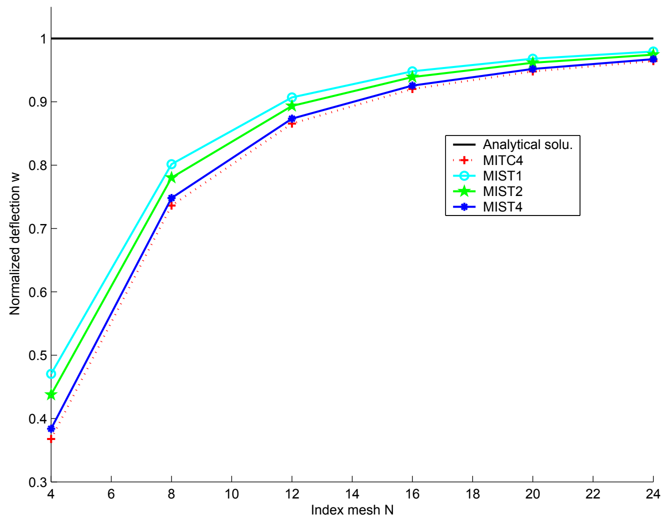

Figure 5: The convergence of deflection at under the load for a regular mesh

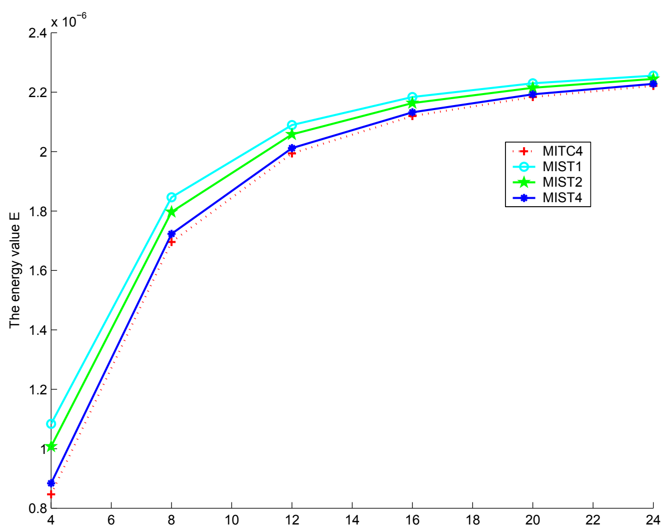

Figure 6: The convergence of strain energy for regular mesh

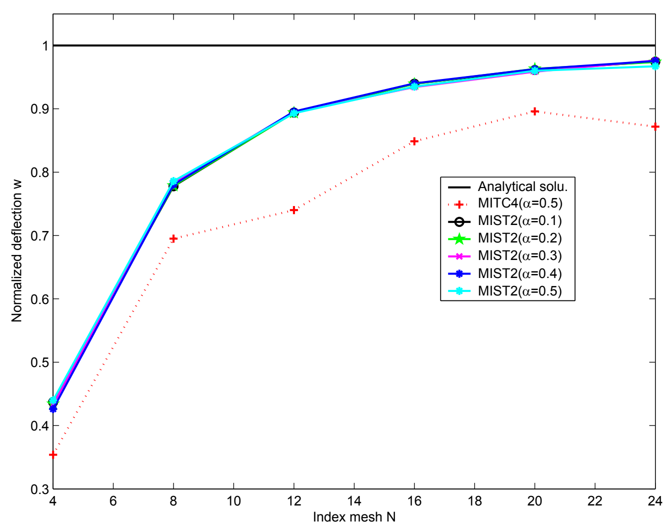

Figure 7: The convergence of deflection for a irregular meshes

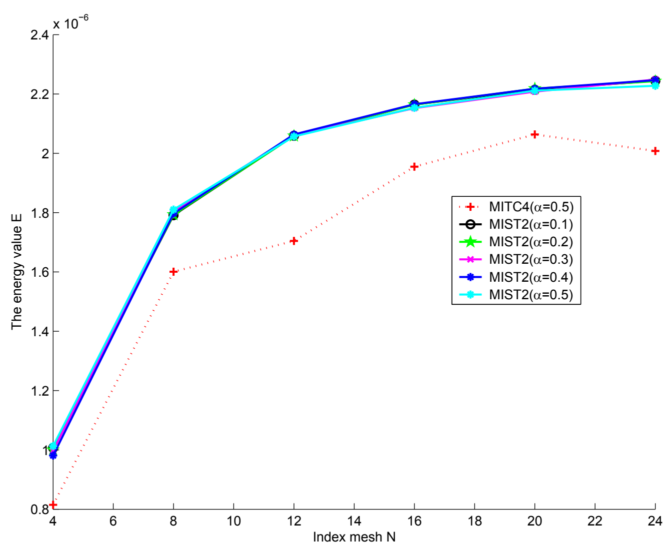

Figure 8: The convergence of strain energy for a irregular meshes

4.1.2 Partly clamped hyperbolic paraboloid

We consider the partly clamped hyperbolic paraboloid shell structure, loaded by self-weight and clamped along one side. The geometric, material and load data are given in figure 9, and only one half of the surface needs to be considered in the analysis.
For this problem there is no analytical solution, and reference values for the total strain energy E and vertical displacement w present in table 5, previously obtained by [20].

Table 5: The reference values for the total strain energy E and vertical displacement w at point B ($x = L/2, y = 0$)

t/L	Strain energy $E(N.m)$	Displacement $w(m)$
$1/1000$	1.1013×10^{-2}	-6.3941×10^{-3}
$1/10000$	8.9867×10^{-2}	-5.2988×10^{-1}

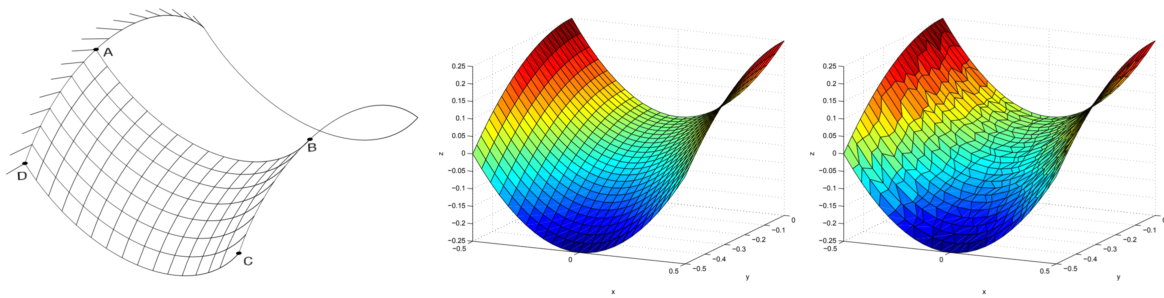

(a) Clamped hyperbolic paraboloid (b) Regular meshes (c) Irregular meshes

Figure 9: Partly clamped hyperbolic paraboloid ($L = 1m$, $E = 2 \times 10^{11} N/m^2$, $\nu = 0.3$, $\rho = 8000kg/m^3$, $z = x^2 - y^2$, $x \in [-0.5, 0.5]$, $y \in [-0.5, 0.5]$)

Table 6: Displacement at point B for a regular mesh(t/L=1/1000)

Mesh N^o	MITC4	MITC16 [20]	Present elements		
			MIST1	MIST2	MIST4
8×4	4.7581e-3	-	5.5858e-3	4.9663e-3	4.8473e-3
16×8	5.8077e-3	-	6.1900e-3	5.9294e-3	5.8624e-3
32×16	6.1904e-3	-	6.3470e-3	6.2487e-3	6.2180e-3
40×20	6.2539e-3	-	6.3691e-3	6.2982e-3	6.2751e-3
48×24	6.2939e-3	6.3941e-3	6.3829e-3	6.3287e-3	6.3108e-3

Figure 10 and figure 11 illustrate the convergence of deflection at point B and strain energy error for a regular mesh with ratio t/L=1000,t/L=1/10000, respectively. In table 6 we have compared the displacement at at point B for a regular mesh of our element to other elements in the literature. We note that the MISTk elements are always more accurate compared to the elements compared with. The results for the distorted meshes are illustrated in figure 12 and table 8.

Table 7: Displacement at point B for a regular mesh(t/L=1/10000)

Mesh N^o	MITC4	MITC16 [20]	Present elements		
			MIST1	MIST2	MIST4
8×4	0.2851	-	0.3398	0.2959	0.2899
16×8	0.4360	-	0.4789	0.4453	0.4401
32×16	0.4967	-	0.5169	0.5021	0.4991
40×20	0.5063	-	0.5214	0.5106	0.5085
48×24	0.5121	0.5298	0.5240	0.5157	0.5137

Table 8: Displacement at point B for a irregular mesh(t/L=1/1000)

Mesh N^o	MITC4($\alpha = 0.5$)	MIST2				
		$\alpha = 0.1$	$\alpha = 0.2$	$\alpha = 0.3$	$\alpha = 0.4$	$\alpha = 0.5$
8×4	4.6652e-3	5.4683e-3	5.4437e-3	5.4359e-3	5.3768e-3	5.3417e-3
16×8	5.7148e-3	6.1379e-3	6.1285e-3	6.1243e-3	6.1196e-3	6.1075e-3
32×16	5.8184e-3	6.2753e-3	6.2648e-3	6.2617e-3	6.2584e-3	6.2520e-3
40×20	5.9769e-3	6.2891e-3	6.2714e-3	6.2682e-3	6.2574e-3	6.2371e-3
48×24	5.8548e-3	6.2957e-3	6.2826e-3	6.2748e-3	6.2664e-3	6.2440e-3

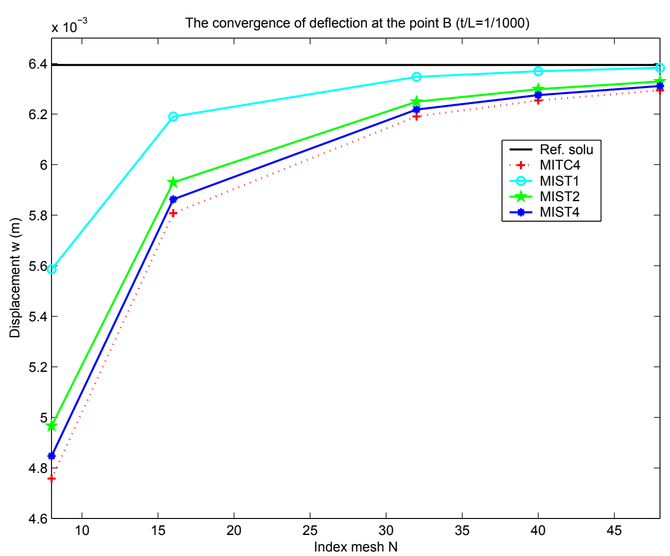

Figure 10: The convergence of deflection of point B for a regular mesh (t/L=1/1000)

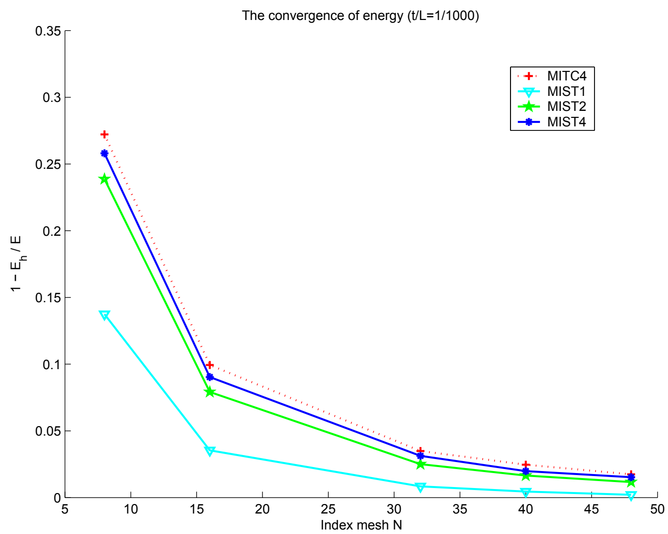

Figure 11: Convergence in strain energy for a regular mesh (t/L=1/1000)

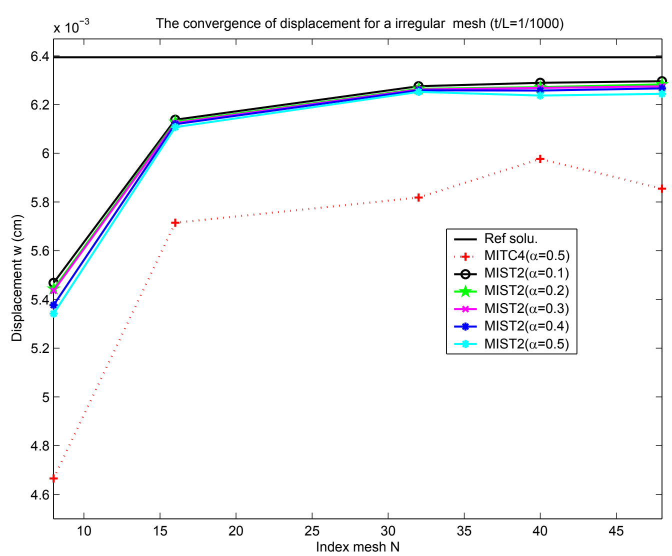

Figure 12: The convergence of deflection of point B for a irregular mesh (t/L=1/1000)

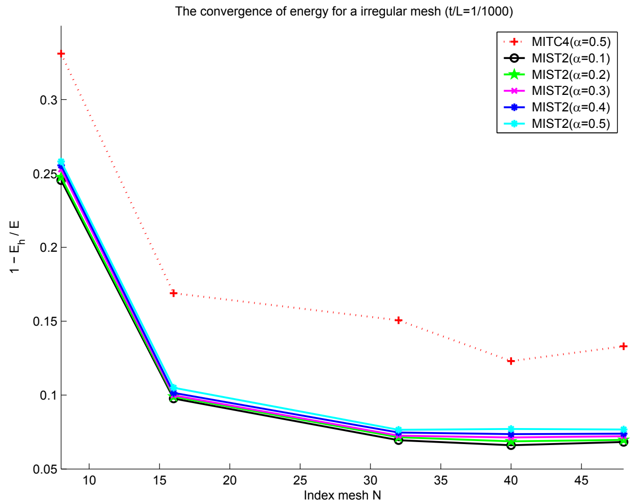

Figure 13: Convergence in strain energy for a irregular mesh (t/L=1/1000)

4.2 Free vibration analysis

4.2.1 A cylindrical shell panel

In this example, a clamped cylindrical shell panel is analyzed. The geometry of the shell is illustrated in figure 14 and its mesh. The following parameters are used in the analysis: length $L = 7.62cm$, radius $R = 76.2cm$, thickness $t = 0.033cm$, elastic modulus $E = 6.8948 \times 10^{10} N/m^2$, Poisson ratio $\nu = 0.33$ and mass density $\rho = 2657.3kg/m^3$. The central subtended angle of the section is $\theta = 7.64^0$. This problem was studied repeatedly in the literature: experimentally by Nath [28], numerically by the extended Rayleigh-Ritz method (ERR) in [34], using triangular finite elements (FET) in [33], analytically by a higher order theory in [24] and with a nine-node assumed natural degenerated shell element in [21]. To analyze the effectiveness of the present method for distorted meshes, we calculate frequencies using 8×8, 12×12, 16×16, and 20×20 meshes for both regular and distorted elements. The first eight frequencies of the clamped cylindrical shell panel are shown in table 9 for regular. The frequencies obtained using the MISTk element are lower than those obtained using the MITC4 element, which is consistent with the fact that strain smoothing leads to softer responses in the case of bilinear interpolants (see, e.g. [32, 29]). Figure 15 illustrate six shape modes of free vibration of the clamped cylindrical shell panel with regular meshes and for distorted meshes.

4.2.2 Hemispherical panel CCFF

Let us consider a hemispherical panel as shown in figure 16 with radius $R = 1$m, thickness $t = 0.1$m, $\varphi_0 = 30^0, \varphi_1 = 90^0, \psi = 120^0$. The material parameters are: Young's modulus $E = 2.1 \times 10^{11} Pa$, Poisson's ratio $\nu = 0.3$, mass density $\rho = 7800kg/m^3$. The first eight frequencies obtained with MITC4 and MISTk elements are given in table 10. The results of both MITC4 and MISTk are compared with the Generalized Differential Quadrature (GDQ) method of [11] and with results obtained using commercial software packages such as Abaqus, Ansys, Nastran, Straus [11]. It is observed that the solutions of the MISTk element are closer to the reference values than the MITC4 element. The first six eigenmodes of hemispherical panels are given in figure 17.

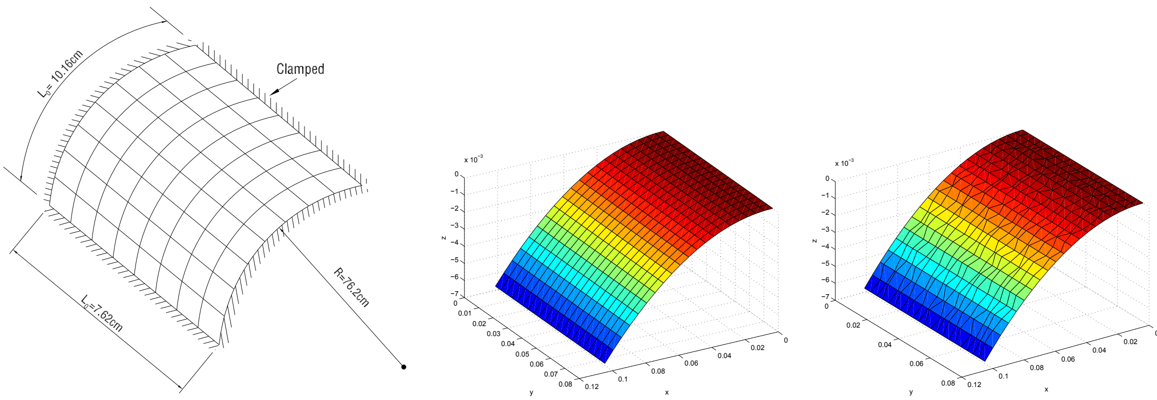

(a) Cylindrical shell panel (b) Regular meshes (c) Distorted meshes

Figure 14: Cylindrical shell panel CCCC: ($E = 6.8948 \times 10^{10} N/m^2$, $\nu = 0.33$, $\rho = 2657.3 kg/m^3$)

Table 9: First eight frequencies of clamped cylindrical shell panel for a regular mesh

Modes	mode 1	mode 2	mode 3	mode 4	mode 5	mode 6	mode 7	mode 8
MITC4	899.34	993.14	1439.03	1476.10	1487.88	1897.88	2496.93	2571.05
	849.72	951.66	1315.32	1365.06	1384.48	1683.56	2009.36	2188.12
	833.42	934.60	1271.52	1340.20	1350.30	1617.52	1848.14	2097.67
	826.09	926.21	1253.18	1328.74	1334.82	1588.41	1780.96	2058.23
MIST1	888.13	980.04	1399.66	1444.49	1454.61	1818.21	2436.97	2490.22
	844.77	945.76	1306.53	1347.22	1365.03	1650.67	1996.11	2159.51
	830.62	931.24	1266.68	1330.04	1339.15	1599.10	1841.04	2081.10
	824.29	924.04	1250.11	1322.18	1327.60	1576.59	1776.50	2047.46
MIST2	892.05	985.36	1416.70	1460.68	1462.96	1847.83	2463.57	2521.81
	846.41	947.99	1309.88	1354.52	1371.65	1661.89	2001.18	2171.50
	831.52	932.47	1268.51	1334.07	1342.77	1605.12	1843.68	2087.84
	824.86	924.82	1251.27	1324.73	1329.88	1580.37	1778.13	2051.77
MIST4	896.76	990.01	1429.84	1470.99	1478.56	1880.34	2483.34	2554.94
	848.54	950.23	1313.19	1360.80	1380.07	1676.05	2006.15	2181.42
	832.74	933.78	1270.34	1337.74	1347.68	1613.18	1846.40	2093.71
	825.65	925.68	1252.42	1327.13	1333.09	1585.58	1779.86	2055.62
Ref.solu.:								
Olson [33]	869.56	957.56	1287.56	1363.21	1440.26	1755.59	1779.63	2056.08
Petyt [34]	890	973	1311	1371	1454	1775	1816	2068
Lim [24]	870	958	1288	1364	1440	1753	1779	2055
Lee [21]	878.253	966.97	1300.51	1377.21	1453.50	1768.54	1797.46	2077.21
Nath [28]	814	940	1260	1306	1452	1802	1735	2100

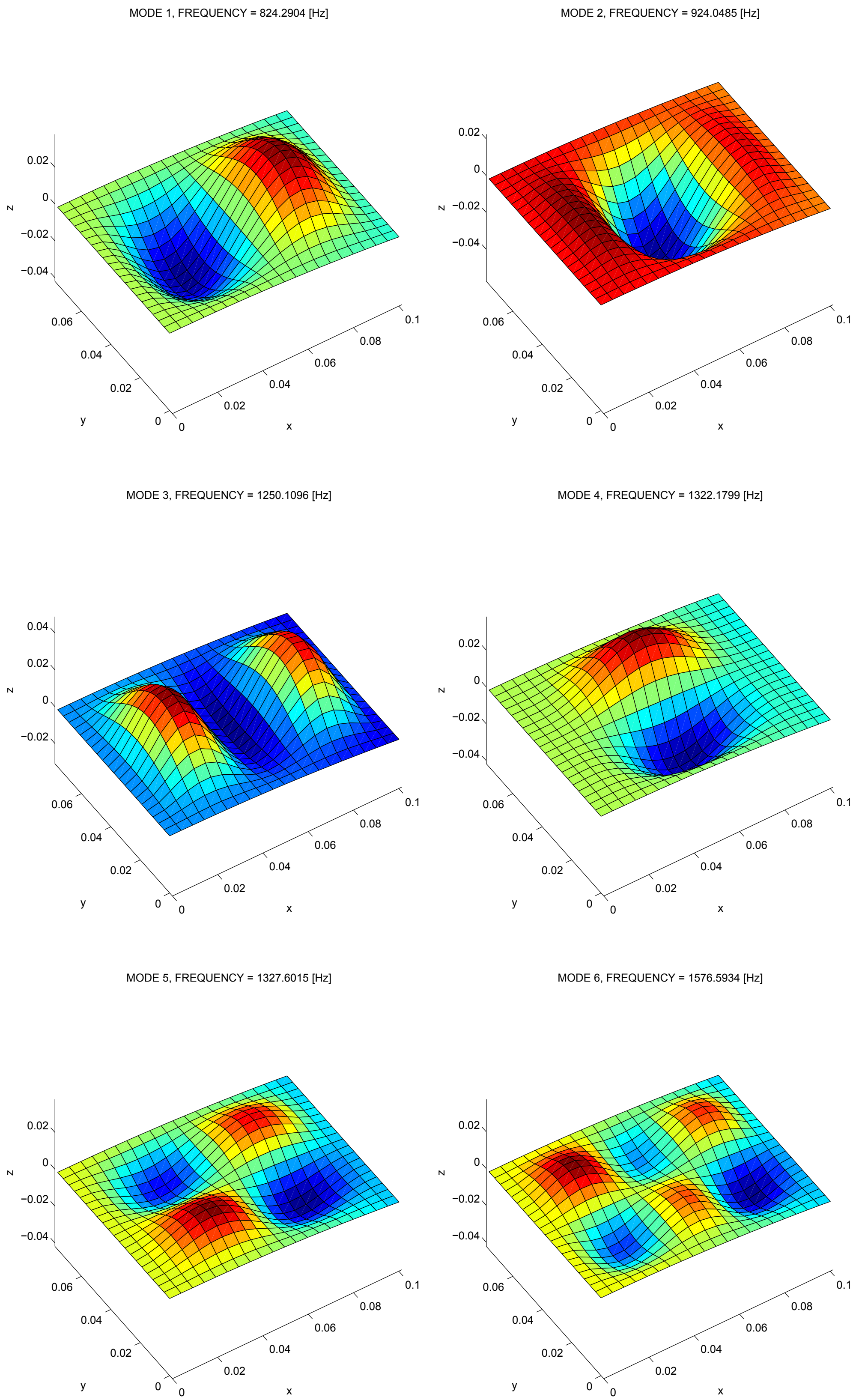

Figure 15: Mode shapes of a clamped cylindrical panel for a regular mesh

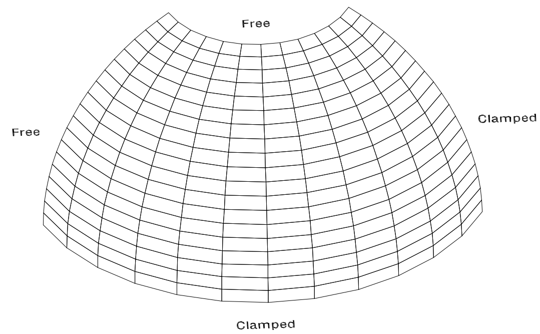

Figure 16: Hemispherical panel CCFF: $R = 1m, h = 0.1m, \varphi_0 = 30^o, \varphi_1 = 90^o, \psi = 120^o$

Table 10: First eight frequencies of hemispherical panel CCFF

Modes	mode 1	mode 2	mode 3	mode 4	mode 5	mode 6	mode 7	mode 8
MITC4	329.23	463.92	726.69	946.05	1089.64	1373.59	1397.38	1503.95
	330.37	463.15	722.32	918.96	1073.88	1340.33	1355.33	1455.62
	330.45	462.65	719.89	908.94	1067.79	1319.45	1344.54	1437.55
	330.34	462.26	718.42	904.07	1064.62	1308.89	1338.90	1428.54
MIST1	310.29	450.94	692.38	917.08	981.27	1047.06	1316.45	1363.52
	323.04	457.50	708.89	907.29	1058.76	1244.61	1321.24	1338.48
	326.67	459.62	712.95	902.60	1060.50	1309.87	1334.86	1426.94
	328.04	460.41	714.19	900.07	1060.39	1302.90	1332.86	1422.39
MIST2	322.17	458.89	714.11	932.60	1071.32	1355.41	1384.53	1474.95
	327.36	460.74	716.95	913.02	1066.87	1333.54	1348.63	1444.90
	328.82	461.38	717.00	905.59	1064.21	1315.82	1340.74	1432.30
	329.33	461.41	716.63	901.91	1062.47	1306.58	1336.50	1425.43
MIST4	326.12	461.83	721.56	940.60	1082.61	1364.10	1391.01	1493.23
	328.92	462.07	719.82	916.46	1070.96	1336.25	1351.96	1451.27
	329.64	462.02	718.46	907.51	1066.24	1317.24	1342.48	1435.28
	329.82	461.86	717.50	903.14	1063.67	1307.47	1337.56	1427.14
Abaqus [11]	326.94	459.01	706.98	884.09	1047.62	1270.77	1309.19	1383.72
Ansys [11]	328.48	460.89	710.52	893.51	1056.12	1285.21	1327.96	1403.99
Nastran [11]	328.69	460.93	711.09	892.71	1055.81	1282.41	1325.89	1401.91
Straus [11]	327.28	458.54	706.64	888.86	1049.49	1278.91	1313.90	1395.46
GDQ [11]	327.39	458.58	705.71	885.18	1046.55	1270.72	1305.12	1382.81

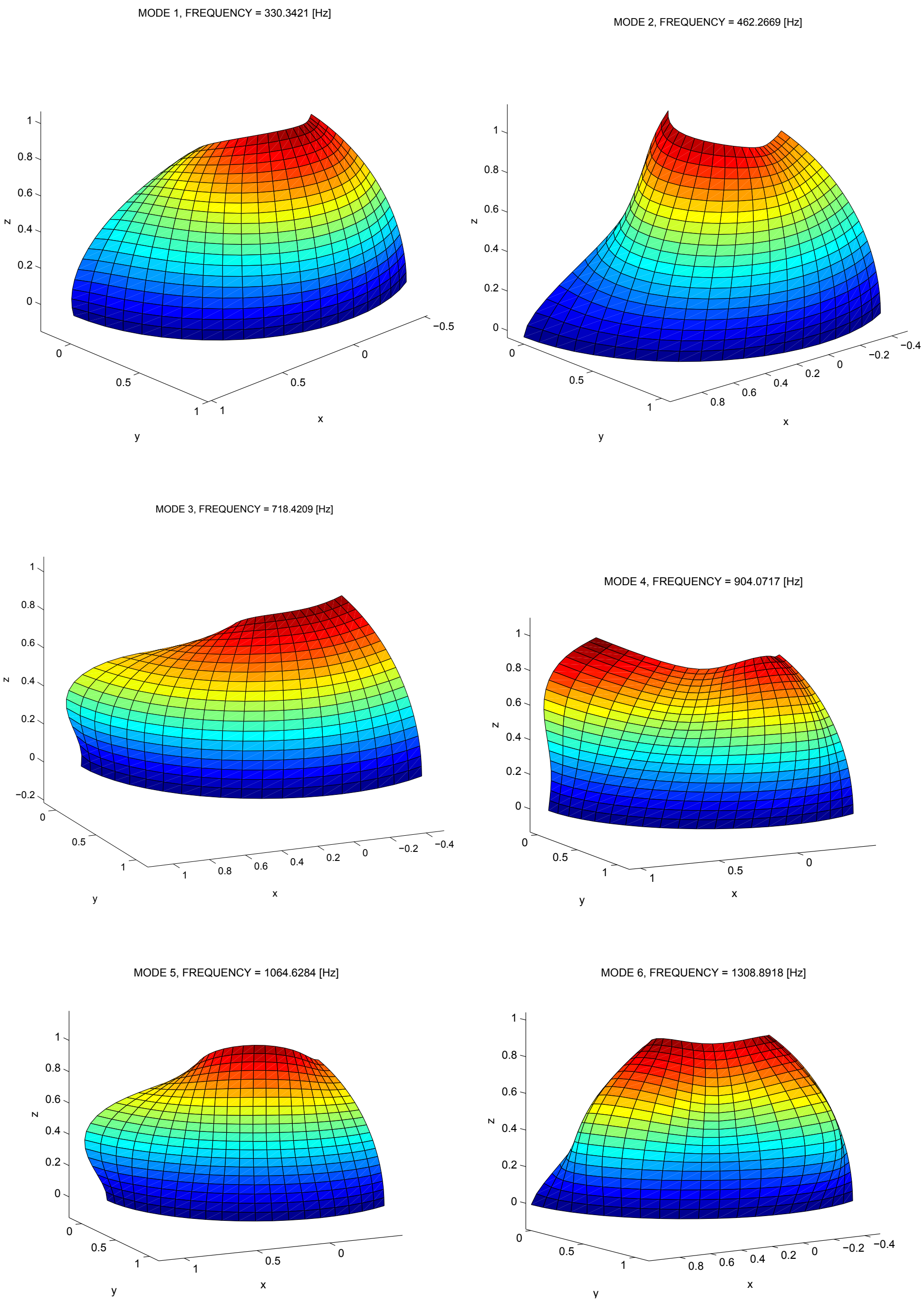

Figure 17: Mode shapes of a hemispherical panel CCFF

5 CONCLUSIONS

In this paper, a smoothed finite element method (SFEM) was further developed for static and free vibration analysis of shell structures. The present method is derived from the linear combination of the gradient smoothing technique and an independent interpolation of assumed natural strains as given in the MITC4 element.

The major advantage of the method, emanating from the fact that the membrane and bending stiffness matrix are evaluated on element boundaries instead of on their interiors is that the proposed formulation gives very accurate and convergent results for distorted meshes.

In addition to the above points, the author believes that the strain smoothing technique herein is seamlessly extendable to complex shell problems such as non-linear material and geometric non-linearities, problems where large mesh-distortion play a major role. Providing an association of boundary integration with partition of unity methods in the extended finite element method [5] may be an interesting subject for improving discontinuous approximations.

REFERENCES

[1] K.J. Bathe. *Finite element procedures*. Englewood Cliffs, NJ: Prentice-Hall, Massachusetts (MIT), 1996.

[2] K.J. Bathe and E.N. Dvorkin. A four-node plate bending element based on Mindlin/Reissner plate theory and a mixed interpolation. *International Journal for Numerical Methods in Engineering*, 21:367 – 383, 1985.

[3] K.J. Bathe and E.N. Dvorkin. A formulation of general shell elements - the use of mixed interpolation of tensorial components. *International Journal for Numerical Methods in Engineering*, 22:697 – 722, 1986.

[4] T. Belytschko and I. Leviathan. Physical stabilization of the 4-node shell element with one-point quadrature. *Computer Methods in Applied Mechanics and Engineering*, 113:321–350, 1994.

[5] S. Bordas, T. Rabczuk, H. Nguyen-Xuan, P. Nguyen Vinh, S. Natarajan, T. Bog, Q. Do Minh, and H. Nguyen Vinh. Strain smoothing in FEM and XFEM. *Computers and Structures*, in press:doi:10.1016/j.compstruc.2008.07.006, 2008.

[6] S. Bordas, T. Rabczuk, and G. Zi. Three-dimensional crack initiation, propagation, branching and junction in non-linear materials by an extended meshfree method without asymptotic enrichment. *Engineering Fracture Mechanics*, 75(5):943–960, 2008.

[7] R. P. R. Cardoso, J. W. Yoon, M. Mahardika, S. Choudhry, R. J. A. Sousa, and R. A. F. Valente. Enhanced assumed strain (EAS) and assumed natural strain (ANS) methods for one-point quadrature solid-shell elements. *International Journal for Numerical Methods in Engineering*, page DOI: 10.1002/nme.2250, 2007. in press.

[8] R. P. R. Cardoso, J. W. Yoon, and R. A. F. Valente. A new approach to reduce membrane and transverse shear locking for one-point quadrature shell elements: linear formulation. *International Journal for Numerical Methods in Engineering*, 66:214–249, 2006.

[9] J.S. Chen, C.T. Wu, S. Yoon, and Y. You. A stabilized conforming nodal integration for Galerkin mesh-free methods. *International Journal for Numerical Methods in Engineering*, 50:435–466, 2001.

[10] E. N. Dvorkin and K. J. Bathe. A continuum mechanics based four-node shell element for general nonlinear analysis. *Engineering Computations*, 1:77–88, 1994.

[11] T. Francesco and V. Erasmo. Vibration analysis of spherical structural elements using the gdq method. *Computers and Mathematics with Applications*, 53:1538–1560, 2007.

[12] P. L. Gould. *Analysis of Shells and Plates*. Springer-Verlag, New York, 1988.

[13] E. Hinton. *Numerical Methods and Software for Dynamic Analysis of Plates and Shells*. Pineridge Press-Swansea,, U.K, 1988.

[14] B.Z. Huang, V.B. Shenoy, and S.N. Atluri. A quasi-conforming triangular laminated composite shell element based on a refined 1st-order theory. *Computational Mechanics*, 13(4):295–314, 1994.

[15] T. J. R. Hughes and T. Tezduyar. Finite elements based upon Mindlin plate theory with particular reference to the four-node isoparametric element. *Journal of Applied Mechanics*, 48:587–596, 1981.

[16] T.J.R. Hughes. *The Finite Element Method*. Prentice-Hall, Englewood Cliffs, NJ, 1987.

[17] T.J.R. Hughes, M. Cohen, and M. Haroun. Reduced and selective integration techniques in finite element method of plates. *Nuclear Engineering Design*, 46:203 – 222, 1978.

[18] T.J.R Hughes and W.K. Liu. Nonlinear finite element analysis of shells. part ii: Two dimensional shells. *Computer Methods in Applied Mechanics and Engineering*, 27:167–182, 1981.

[19] T.J.R. Hughes, R.L. Taylor, and W. Kanoknukulchai. Simple and efficient element for plate bending. *International Journal for Numerical Methods in Engineering*, 11:1529 – 1543, 1977.

[20] D. Chapelle K.J. Bathe, A. Iosilevich. An evaluation of the mitc shell elements. *Computers and Structures*, 75:1–30, 2000.

[21] S. J. Lee and S. E. Han. Free-vibration analysis of plates and shells with a nine-node assumed natural degenerated shell element. *Journal of Sound and Vibration*, 4:605–633, 2001.

[22] A. W. Leissa. *Vibration of Shell*. NASA, SP-288,Washington DC, 1973.

[23] A.W Leissa. Vibration of plates. *NASA SP-160*, 1969.

[24] C. W. Lim and K. M. Liew. A higher order theory for vibration of shear deformable cylindrical shallow shells. *International Journal of Mechanical Sciences*, 37:277–295, 1995.

[25] G. R. Liu, K. Y. Dai, and T. T. Nguyen. A smoothed finite element for mechanics problems. *Computational Mechanics*, 39:859–877, 2007.

[26] G. R. Liu, T. T. Nguyen, K. Y. Dai, and K. Y. Lam. Theoretical aspects of the smoothed finite element method (sfem). *International Journal for Numerical Methods in Engineering*, 71:902–930, 2007.

[27] R. D. Mindlin. Influence of rotary inertia and shear in flexural motion of isotropic, elastic plates. *Journal of Applied Mechanics*, 18:1031–1036, 1951.

[28] J. M. Deb Nath. Dynamics of rectangular curved plates. *Ph.D. Thesis, University of Southampton*, 1969.

[29] N. Nguyen-Thanh, T. Rabczuk, H. Nguyen-Xuan, and S. Bordas. A smoothed finite element method for shell analysis. *Computer Methods in Applied Mechanics and Engineering*, 198:165–177, 2008.

[30] H. Nguyen-Xuan, S. Bordas, and H. Nguyen-Dang. Smooth finite element methods: Convergence, accuracy and properties. *International Journal for Numerical Methods in Engineering*, page DOI: 10.1002/nme.2146, 2007. in press.

[31] H. Nguyen-Xuan, T. Rabczuk, S. Bordas, and J. F. Debongnie. A smoothed finite element method for plate analysis. *Computer Methods in Applied Mechanics and Engineering*, 197:1184–1203, 2008.

[32] H. Nguyen-Xuan, T. Rabczuk, S. Bordas, and J. F. Debongnie. A smoothed finite element method for plate analysis. *Computer Methods in Applied Mechanics and Engineering*, 197:1184–1203, 2008.

[33] M. D. Olson. Dynamic analysis of shallow shells with a doubly-curved triangular finite element. *Journal of Sound and Vibration*, 3:299–318, 1971.

[34] M. Petyt. Vibration of curved plates. *Journal of Sound and Vibration*, 15:381–395, 1971.

[35] T. H. H. Pian and C. C. Wu. *Hybrid and Incompatible finite element methods*. CRC Press, Boca Raton, 2006.

[36] T. Rabczuk and P. Areias. A meshfree thin shell for arbitrary evolving cracks based on an external enrichment. *Computer Modeling in Engineering and Sciences*, 16(2):115–130, 2006.

[37] T. Rabczuk, P.M.A. Areias, and T. Belytschko. A meshfree thin shell for large deformation, finite strain and arbitrary evolving cracks. *International Journal for Numerical Methods in Engineering*, 72(5):524–548, 2007.

[38] E. Reissner. The effect of transverse shears deformation on the bending of elastic plate. *Journal of Applied Mechanics*, 12:69–76, 1945.

[39] J. M. A. César De Sá, R. M. N. Jorge, R. A. F. Valente, and P. M. A. Areias. Development of shear locking-free shell elements using an enhanced assumed strain formulation. *International Journal for Numerical Methods in Engineering*, 53:1721–1750, 2002.

[40] J.C. Simo, D.D. Fox, and M.S. Rifai. On a stress resultant geometrically exact shell model. part ii: The linear theory; computational aspects. *Computer Methods in Applied Mechanics and Engineering*, 73:53–92, 1989.

[41] J.C. Simo and M.S. Rifai. A class of mixed assumed strain methods and the method of incompatible modes. *International Journal for Numerical Methods in Engineering*, 29:1595 – 1638, 1990.

[42] J. Sladek, V. Sladek, P. Solek, P.H. Wen, and S.N. Atluri. Thermal analysis of Reissner-Mindlin shallow shells with FGM properties by the MLPG. *Computer Modeling in Engineering and Sciences*, 30(2):77–97, 2008.

[43] Y. Suetake, M. Iura, and S.N. Atluri. Variational formulation and symmetric tangent operator for shells with finite rotation field. *Computer Modeling in Engineering and Sciences*, 4(2):329–336, 2004.

[44] R.L. Taylor and Kasperm E. P. A mixed-enhanced strain method. *Computers and Structures*, 75:237–250, 2000.

[45] S. P. Timoshenko and S. Woinowsky-Krieger. *Theory of Plates and Shells(2nd edn)*. McGraw-Hill, New York, 1959.

[46] O.C. Zienkiewicz and R.L. Taylor. *The Finite Element Method*. 5th Edition, Butterworth Heinemann, Oxford, 2000.

[47] O.C. Zienkiewicz, R.L. Taylor, and J.M. Too. Reduced intgration technique in general analysis of plates and shells. *International Journal for Numerical Methods in Engineering*, 3:275 – 290, 1971.